Received: 21 January 2023 | Revised: 10 October 2023 | Accepted: 3 December 2023

DOI: 10.1002/pip.3761

RESEARCH ARTICLE

PROGRESS IN PHOTOVOLTAICS WILEY

Dipoles and defects caused by CO_2 plasma improve carrier transport of silicon solar cells

Shenglei Huang[1,2,3] | Yuhao Yang[1] | Junjun Li[4] | Kai Jiang[1,3] | Xiaodong Li[1,3] | Yinuo Zhou[1,3] | Zhenfei Li[1] | Guangyuan Wang[1] | Qiang Shi[1] | Jianhua Shi[1] | Junlin Du[1] | Anjun Han[1,5] | Jian Yu[4] | Fanying Meng[1,3] | Liping Zhang[1,3] | Zhengxin Liu[1,2,3] | Wenzhu Liu[1,3]

[1]Research Center for New Energy Technology (RCNET), National Key Laboratory of Materials for Integrated Circuits, Shanghai Institute of Microsystem and Information Technology (SIMIT), Chinese Academy of Sciences (CAS), Shanghai, People's Republic of China

[2]School of Physical Science and Technology, ShanghaiTech University, Shanghai, People's Republic of China

[3]University of Chinese Academy of Sciences (UCAS), Beijing, People's Republic of China

[4]School of New Energy and Materials, Southwest Petroleum University, Chengdu, People's Republic of China

[5]Science and Technology on Micro-system Laboratory, Shanghai Institute of Microsystem and Information Technology (SIMIT), Chinese Academy of Sciences (CAS), Shanghai, People's Republic of China

Correspondence
Zhengxin Liu and Wenzhu Liu, Shanghai Institute of Microsystem and Information Technology (SIMIT), Chinese Academy of Sciences (CAS), Shanghai 201800 People's Republic of China.
Email: z.x.liu@mail.sim.ac.cn and wenzhu.liu@mail.sim.ac.cn

Funding information
National Natural Science Foundation of China, Grant/Award Numbers: 62004208, T2322028, 62074153; Science and Technology Commission of Shanghai Municipality, Grant/Award Number: 22ZR1473200; Foundation of the Key Laboratory of National Defense for Science and Technology of China, Grant/Award Number: 61428040202; Research on Key technologies of high efficiency ultra-thin heterojunction solar cell and module, Grant/Award Number: HNKJ22-H154

Abstract

Carrier-selective contact is a fundamental issue for solar cells. For silicon heterojunction (SHJ) solar cells, it is important to improve hole transport because of the low doping efficiency of boron in amorphous silicon and the barrier stemming from valence band offset. Here, we develop a carbon dioxide (CO_2) plasma treatment (PT) process to form dipoles and defect states. We find a dipole moment caused by longitudinal distribution of H and O atoms. It improves hole transport and blocks electron transport and thus suppresses carrier recombination. In the meantime, the CO_2 PT process also results in defect states, which reduce passivation performance but improve hole hopping in the intrinsic amorphous layer. As a balance, an appropriate CO_2 PT process at the i/p interface increases fill factor and power conversion efficiency of SHJ solar cells. We emphasize, based on sufficient evidences, this work finds a distinct role of the CO_2 plasma in SHJ solar cells opposed to reported mechanisms.

KEYWORDS
carrier transport, CO_2 plasma, defect states, dipole moments, SHJ solar cells

1 | INTRODUCTION

Silicon heterojunction (SHJ) solar cells have attracted continuous attention due to low-temperature processing, high open-circuit voltage (V_{OC}), high power conversion efficiency (*PCE*), low temperature coefficient, and light-induced performance increase.[1–4] In particular, a world-record *PCE* of 26.8% for SHJ solar cells was achieved in 2022 on a 274.4 cm^2 monocrystalline-silicon (c-Si) wafer.[5,6]

For solar cells, carrier selectivity plays a key role in the device performance. One of the efficient approaches is to modify the work function (*WF*) of materials by forming a dipole. The interfacial dipole causes changes in the band structure and thus regulates carrier transport. Incorporating dipole interlayer has been an important interfacial engineering strategy in organic, polymer, and perovskite solar cells. Feng et al.[7] applied water-alcohol-soluble polyelectrolyte dipole interlayers in single-junction organic solar cells and achieved a *PCE* of

17.6%. Choi et al.[8] reported that the *WF* of ITO increased from 4.77 to 5.02 eV by a dipole interlayer, which contributed to the smooth hole transport of polymer solar cells. Ok et al.[9] investigated the merits of transition dipole moment to the performances of perovskite solar cells. Canil et al.[10] found electron acceptor or donor molecules resulted in the positive or negative *WF* shifted up to several hundreds of milielectron volts. Furthermore, the interfacial dipole is also reported in the research field of SHJ solar cells.[11–13]

Plasma treatment (PT), such as hydrogen (H_2) PT, has been widely studied to improve performance of SHJ solar cells. H_2 PT is generally considered to improve chemical passivation of SHJ solar cell. However, due to the good passivation of the hydrogenated amorphous silicon (a-Si:H) layers, the improvement by this strategy is quite limited, as shown in Table 1.[14–17] In this study, we report that carbon dioxide (CO_2) PT at the i/p interface after the deposition of intrinsic hydrogenated amorphous silicon (i-a-Si:H) injects oxygen (O) atoms to the a-Si:H network and getters hydrogen (H) atoms from the plasma of the subsequent deposition process. We find H atoms are further away from the i-a-Si:H surface in comparison to O atoms. This leads to an interfacial dipole whose positive end pointing towards the p-type hydrogenated amorphous silicon (p-a-Si:H) layer. As a result, the surface WF ($WF_{surface}$) of i-a-Si:H film significantly decreases by about 0.44 eV, and the energy band bends upward. Consequently, the dipole reduces the hole hopping distance and blocks electron transport. In addition, CO_2 PT also causes defect states that improve hole transition[18] but has a slightly negative impact on chemical passivation.[19] We optimized balance CO_2 PT duration for the i/p interface of SHJ solar cells, which boosts their fill factor (*FF*) from 77.61% to 82.37% and *PCE* from 22.16% to 23.59%.

2 | EXPERIMENTAL SECTION

2.1 | Materials

In this study, a-Si:H film was deposited in a plasma enhanced chemical vapor deposition (PECVD) system (ULVAC-CME400), and three different types of a-Si:H film were deposited in independent chambers. The PT process was taken place in the chamber in which doped a-Si:H film was deposited. Each stack would not be exposed to air before production was completed. For Secondary Ion Mass Spectroscopy (SIMS) analyses, c-Si/i-a-Si:H/p-a-Si:H stacks with and without a 20 s CO_2 PT process after the deposition of i-a-Si:H film were prepared. Time of Flight Secondary Ion Mass Spectroscopy (TOF-SIMS) analyses were carried out using a TOF-SIMS 5 spectrometer (ION TOF, GmbH-Muenster, Germany). The analysis chamber was maintained at a pressure of 1×10^{-9} mbar. A pulsed 30 keV Bi^+ primary ion source was employed for analysis at a current of 1.0 pA. Depth profiles were acquired using a Cs^+ sputter beam with 500 eV for H^-, O^-, Si^-, and B^- negative ions under the dual beam mode. Kelvin Probe Force Microscope (KPFM, KEYSIGHT Technologies 7500) measurements were performed to obtain surface potential of c-Si/i-a-Si:H stacks with and without a 20 s CO_2 PT process and a 30 s H_2 PT process. Details of the CO_2 PT process and the H_2 PT process are shown in Table S1. The surface potential is associated with the *WF*, which is determined by contact potential difference (*CPD*) between a Pt-coated conductive cantilever probe and the samples. The WF of Pt-coated tip and sample can be calculated using Equation (1).

$$CPD = \left(\Phi_{tip} - \Phi_{sample}\right)/e, \tag{1}$$

where Φ_{tip} is the *WF* of the tip, Φ_{sample} is the *WF* of the sample surface, and *e* is the elementary charge of electron. Herein, the *WF* of the Pt/Cr-coated tip was calibrated with the HOPG sample ($\Phi_{HOPG} = 4.6$ eV, $CPD = 420$ mV). Therefore, the Φ_{tip} is 5.02 eV. The Φ_{sample} can be calculated using Equation (2):

$$\Phi_{sample} = \Phi_{tip} - e \times CPD. \tag{2}$$

For ultraviolet photoelectron spectroscopy (UPS, Thermo Fisher, ESCALAB 250Xi) measurements, c-Si/i-a-Si:H stacks without PT (REF), with a CO_2 PT process, and with a H_2 PT process after the CO_2 PT process were prepared, respectively. For Fourier-Transform Infrared spectroscopy (FTIR, Perkin Elmer, Spectrum 100) measurements, i-a-Si:H and p-a-Si:H thin films (with and without a 20 s CO_2 PT) were deposited on >3,000 Ωcm float-zone c-Si substrates, and their infrared absorptions were characterized using the transmission mode. The crystallinity of p-a-Si:H film was probed by Raman spectroscopy (WITEC alpha 300R) with a wavelength of 532 nm. Moreover, the dark conductivity was measured through Keithley 6487 at 25°C. The minority carrier lifetime (τ_{eff}) and implied V_{OC} (iV_{OC}) of semi-cells (SHJ solar cells without finger and bus bars) were conducted with a Sinton WCT-120. Schematics of samples for measurements are shown in Figure S1.

TABLE 1 Improvements in V_{OC} and *FF* through the H_2 PT reported by researchers.

	i-p (a)[14]	i-p (b)[15]	i-n[16]	Both sides[17]
V_{OC} w/o H_2 PT (mV)	724	~721	722	734.5
V_{OC} with H_2 PT (mV)	729	~722	728	736.1
$\triangle V_{OC}$ (mV)	5	~1	6	1.6
FF w/o H_2 PT (%)	70.2	~72	78.5	77.23
FF with H_2 PT (%)	71.3	~73	79.4	77.32
$\triangle FF$ (%)	1.1	~1	0.9	0.09

2.2 | Devices

The architecture of 6-in. rear-emitter SHJ solar cells are shown in Figure 4B. N-type c-Si (100) wafers (150 μm, 156 × 156 mm^2, resistivity: 0.3–2.1 Ωcm) were textured with KOH, followed by the standard Radio Corporation of America (RCA) cleaning process, and subsequently dipped in 2% diluted HF for 1 min. Intrinsic and doped a-Si:H films were deposited on both sides of the wafers, and some

samples underwent a CO_2 PT process after the deposition of i-a-Si:H film. After the deposition of doped a-Si:H film, the tungsten-doped indium oxide (IWO) layers were deposited by the reactive plasma deposition (RPD) technique. Subsequently, the Ag electrodes were screen-printed with conventional busbar and finger patterns on the IWO layers. The completed solar cells were characterized by standard 1-Sun light current–voltage (I-V test in-house built setup with a Yamashita class AAA light simulator at 1.5 air mass). Pseudo fill factor (p*FF*) was measured by the Sinton WCT-120 with Suns-Voc. Electrochemical impedance spectroscopy (EIS) measurements were carried out by Bio-Logic SAS VSP-300 in the dark. Dark *J-V* curves were scanned from −1 to 1 V. Nyquist plots were obtained at a bias of 0.25 V with an amplitude of 5 mV and frequency range from 0.1 Hz to 1 kHz.

3 | RESULTS AND DISCUSSION

3.1 | Dipoles and defects induced by CO_2 PT

By SIMS measurements, Figure 1A shows the H and O distributions in c-Si/i-a-Si:H/p-a-Si:H stacks with (EXP) and without (REF) a 20 s CO_2 PT process after the i-a-Si:H deposition. The CO_2 discharge in PECVD is known to show intense vacuum-ultraviolet irradiation, producing active oxygen species radicals. These radicals oxidize the surface of the sample to form O-rich thin film, so there are more O atoms near the i/p interface. As shown in Figure S2, the SiO stretching mode at 1,044 cm^{-1} (Fourier-transform infrared spectroscopy; FTIR) of the EXP sample confirms the injection of O atoms.[20] Interestingly, H intensity also increases substantially near the i/p interface. The presence of strained Si-O bonds in the O-rich thin film gives rise to an additional channel of interaction of H atoms with film networks.[21] These extra H atoms are possibly from the plasma of SiH_4 and H_2 during the p-a-Si:H deposition.[22] The position of the half peak width of the O and H intensity of the EXP sample is marked in Figure 1A, and it is found that the hydrogen peak is further away from the interface compared to the oxygen peak. Since O is more electronegative than H, local charges are shifted towards O atoms, which causes large dipoles pointing from the i-a-Si:H layer towards the p-a-Si:H layer, as schematic in Figure 1B.

Figure S3 shows the effect of dipoles on the vacuum level and thus $WF_{surface}$. Dipoles (point outside with respect to the i-a-Si:H surface) will shift the local vacuum level downwards and therefore decrease $WF_{surface}$ of film.[23,24] To confirm the formation of the dipole on the i-a-Si:H surface, $WF_{surface}$ of i-a-Si:H film with and without a CO_2 PT process and a H_2 PT process was measured by KPFM. The H_2 PT process after the CO_2 PT process was to mimic the H_2 PT that would occur during the p-a-Si:H deposition. As shown in Figure 1C, the *CPD* of the i-a-Si:H film increases significantly after the PT process, which indicates decrease of $WF_{surface}$. $WF_{surface}$ of i-a-Si:H film before and after the PT process is calculated to be 4.60 and 4.16 eV, respectively, suggesting the PT process decreased $WF_{surface}$ by 0.44 eV. Furthermore, UPS measurements were utilized to investigate the surface electronic states of i-a-Si:H film. The valence band edge curves of the i-a-Si:H film without PT (REF), with a CO_2 PT process and with a H_2 PT process after the CO_2 PT process are shown in Figure S4. The energy difference between the valence band edge (E_V) and the Fermi level (E_F) is 1.30, 1.08, and 1.35 eV, respectively. After CO_2 PT, electronegative O atoms gather on the surface of film, the energy band bends upward since negative charges on the surface, and the $E_F - E_V$ value decreases. After CO_2 PT, a H_2 PT process was carried out. Then, H atoms with weak electronegativity gather on the surface of O-rich film, the energy band bends downward since positive charges on the surface and $E_F - E_V$ value increases. These results also confirm that the PT process causes the existence of dipoles. Figure 1D represents a schematic diagram of the energy bands in the hole-selective contact stack with and without the CO_2 PT treatment. Since the energy band of the i-a-Si:H bends upward due to dipoles pointing from the i-a-Si:H layer towards the p-a-Si:H layer (green lines), there is a higher barrier for electron transport that is beneficial to suppress the charge recombination. The implication on hole transport is discussed in the next section.

Mazzarella et al.[25] and Jiang[26] found that CO_2 PT on the i/p interface of the SHJ solar cells promoted nucleation and improved the conductivity of p-type emitter layer. To study the structural features of p-a-Si:H film, Raman spectra of samples without and with a 20 s CO_2 PT process are shown in Figure S5. Spectra exhibit no changes, demonstrating CO_2 PT does not promote the formation of nanocrystalline phase. Dark current–voltage curve of p-a-Si:H thin film is shown in Figure S6. The curve changes slightly, which indicates that the dark conductivity of p-a-Si:H thin film is hardly improved after CO_2 PT. Our observations are distinctly different from other researches, indicating that there are different mechanisms underlying the impact of CO_2 PT under low pressure on silicon solar cells in this study.

We treated tungsten-doped indium oxide (IWO)/n-type hydrogenated amorphous silicon(n-a-Si:H)/i-a-Si:H/n-c-Si/i-a-Si:H/p-a-Si:H/IWO samples with different CO_2 PT duration on the i-a-Si:H layer at the p-a-Si:H side. Figure 2A,B shows that both τ_{eff} and iV_{OC} decrease slightly with short CO_2 PT duration, τ_{eff} and iV_{OC} of the sample with a 30 s CO_2 PT process decrease significantly compared to that of the REF sample. The pseudo fill factor (p*FF*) characterizes losses due to injection-dependent recombination.[27] Figure 2C shows p*FF* of SHJ solar cells with different CO_2 PT duration before the deposition of the p-a-Si:H layer. Each plot is an average value from three pieces of 6-in. rear-emitter SHJ solar cells (~244 cm^2). Along with the increase of CO_2 PT duration, p*FF* continues to decrease from 84.8% (REF) to 83.03% (30 s). This passivation degradation indicates an increase of defect states.[19] Figure 2D shows the forward dark current density-voltage (*J-V*) characteristics of SHJ solar cells with different CO_2 PT duration. The forward current in SHJ solar cell is dominated by the diffusion current and the tunneling current at higher bias voltage and lower bias voltage, respectively.[28] The tunneling current of cells with a 10 s or 20 s CO_2 PT process is slightly larger than that of the REF cell, but the tunneling current increases significantly when CO_2 PT duration is increased to 30 s. The increase of the tunneling current is caused by the increase of the depletion region recombination and

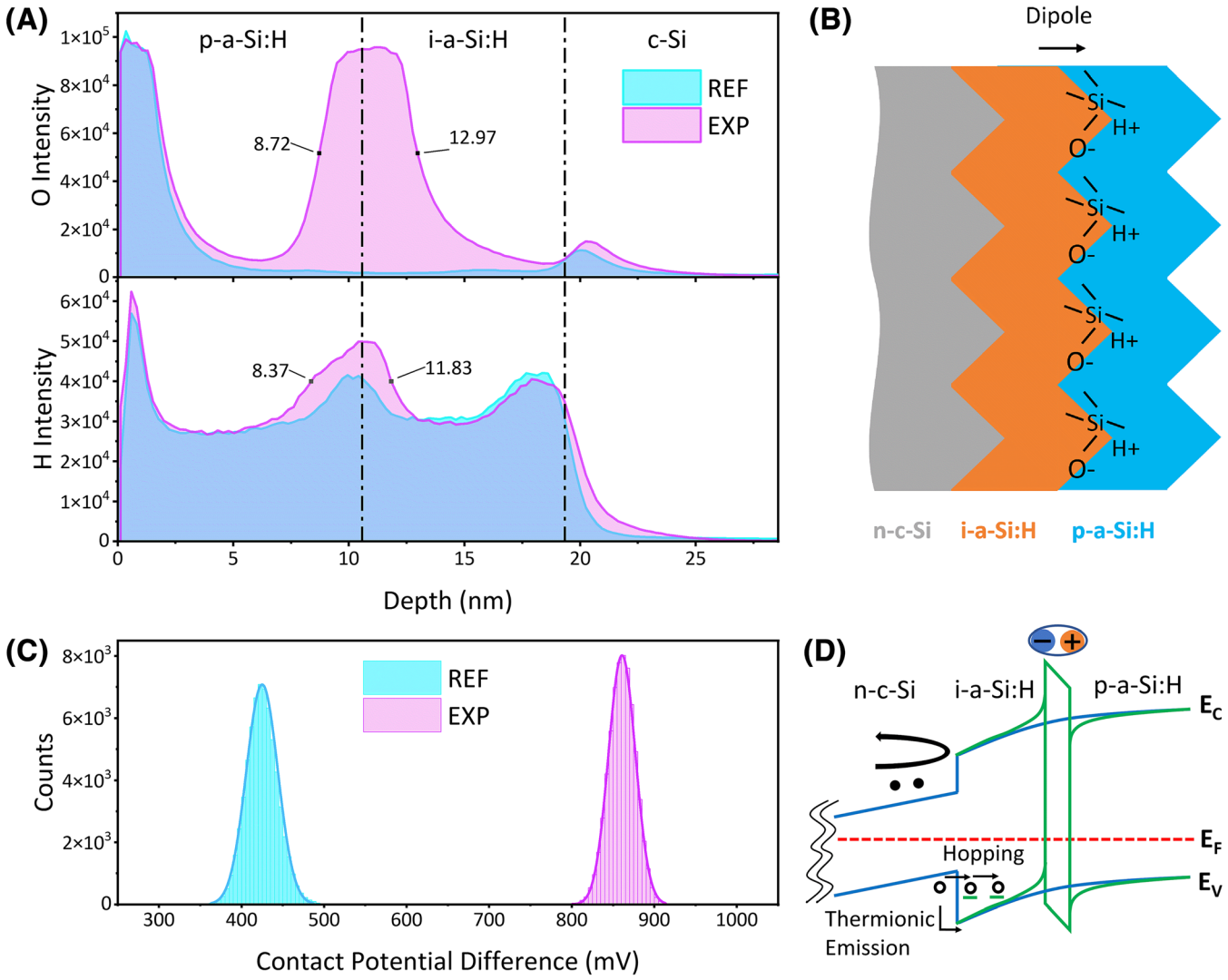

FIGURE 1 (A) Distributions of H and O in c-Si/i-a-Si:H/p-a-Si:H stacks with (EXP) and without (REF) a 20 s CO_2 PT process after the i-a-Si:H deposition. The position of the half peak width of O and H intensity of the EXP sample is marked. (B) Schematic of hole-selective contacts with a CO_2 PT process. (C) Contact potential difference (*CPD*) of i-a-Si:H films before (REF) and after (EXP) a 20 s CO_2 PT process and a 30 s H_2 PT process. (D) Schematics of charge carrier collection at the hole contact without (blue lines) and with (green lines) dipoles.

shunting path within the p-n junction. Figure 2E shows typical Nyquist plots of the SHJ solar cells with different CO_2 PT duration, recorded in the dark at a bias voltage of 0.25 V. The values of the shunt resistivity (R_{sh}) obtained from EC-lab analysis of the EIS data are shown in the inset. R_{sh} decreases with the increase of CO_2 PT duration. This demonstrates longer CO_2 PT increases defect states, carrier recombination, and shunting currents, which will decrease R_{sh} of the device and thus V_{OC} and *FF* to some extent.

3.2 | Performance of SHJ solar cells

To our surprise, these defect states on the other hand also show a positive role. Pradyumna Muralidharan et al.[18,29] claimed that for a SHJ solar cell, charge transport through the i-a-Si:H layer depends on the defect/phonon assisted transport. Holes hop from defect to defect within the i-a-Si:H layer before they are collected. Longer transit times are indicative of photocurrent suppression, which leads to an S-shape behavior in the *J-V* curve of SHJ solar cells. More available defect states reduce the number of phonons required for hole injection into the barrier, thereby reducing the transit time associated with injection and thus reducing the series resistance (R_s). In addition, as shown in Figure 1D, the valence band offset does not seem to change at the c-Si/i-a-Si:H interface, which means the thermionic emission and the direct tunneling are almost unaffected, but the hopping distance reduces as the valence band bends upward, which is also beneficial for hole to hop through the i-a-Si:H layer. The difference between *FF* and p*FF* is a misleading measure of R_s losses.[30] In Figure 3A,B, We plot p*FF* - *FF* and R_s of solar cells prepared with various CO_2 PT duration. They show the same trend. R_s of SHJ solar cells

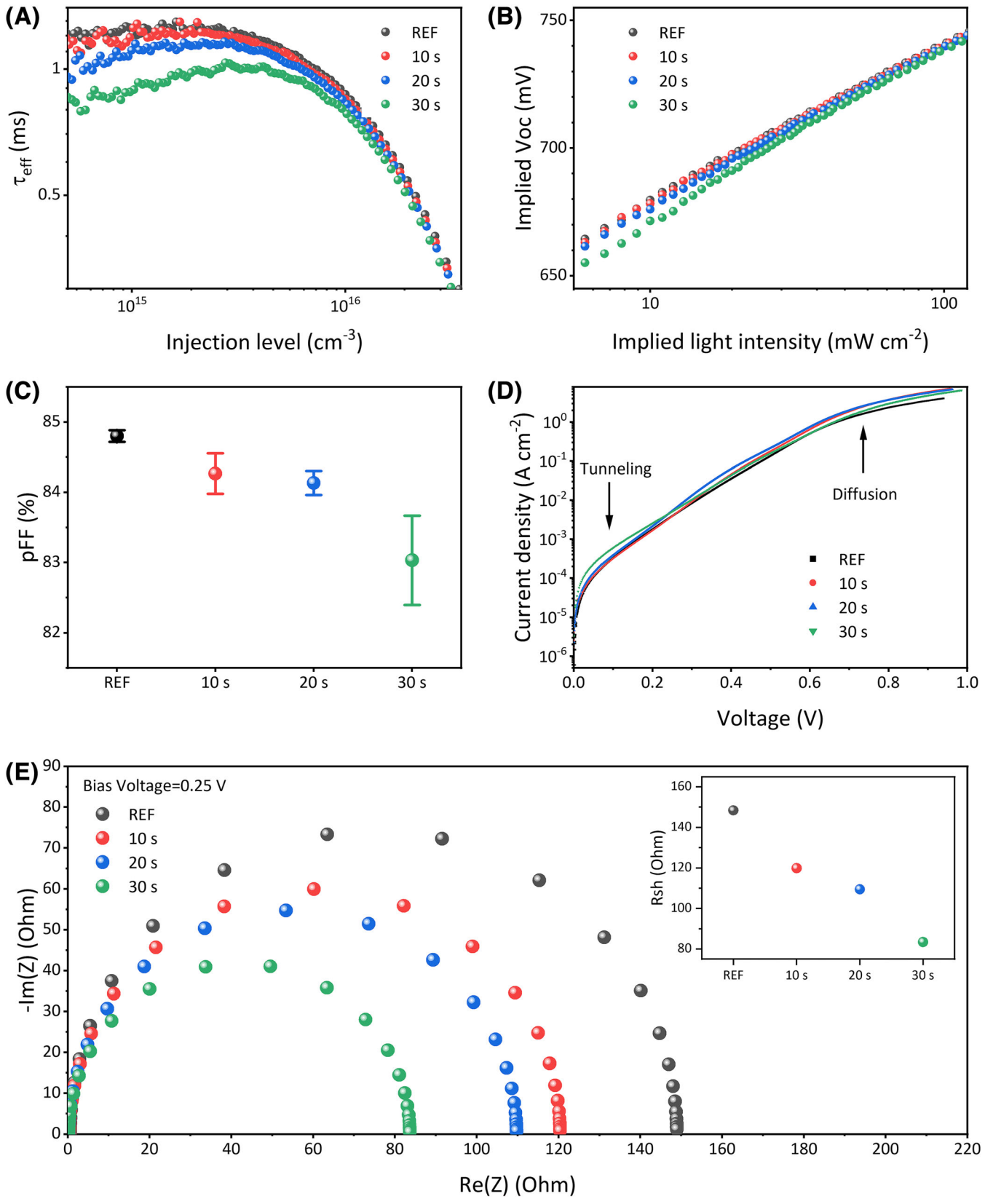

FIGURE 2 (A) Injection-dependent τ_{eff} and (B) implied V_{OC} (iV_{OC}) dependence on implied light intensity of IWO/n-a-Si:H/i-a-Si:H/n-c-Si/i-a-Si:H/p-a-Si:H/IWO with different CO_2 PT duration. (C) Pseudo-*FF* plots and (D) dark *J-V* curve of SHJ solar cells with different CO_2 PT duration. (E) Nyquist plots of electrochemical impedance spectroscopy (EIS) for devices with different CO_2 PT duration in the dark at a bias of 0.25 V. The inset shows the shunt resistance (R_{sh}) at a bias of 0.25 V of SHJ solar cells with different CO_2 PT duration obtained from EC-lab analysis of the EIS data.

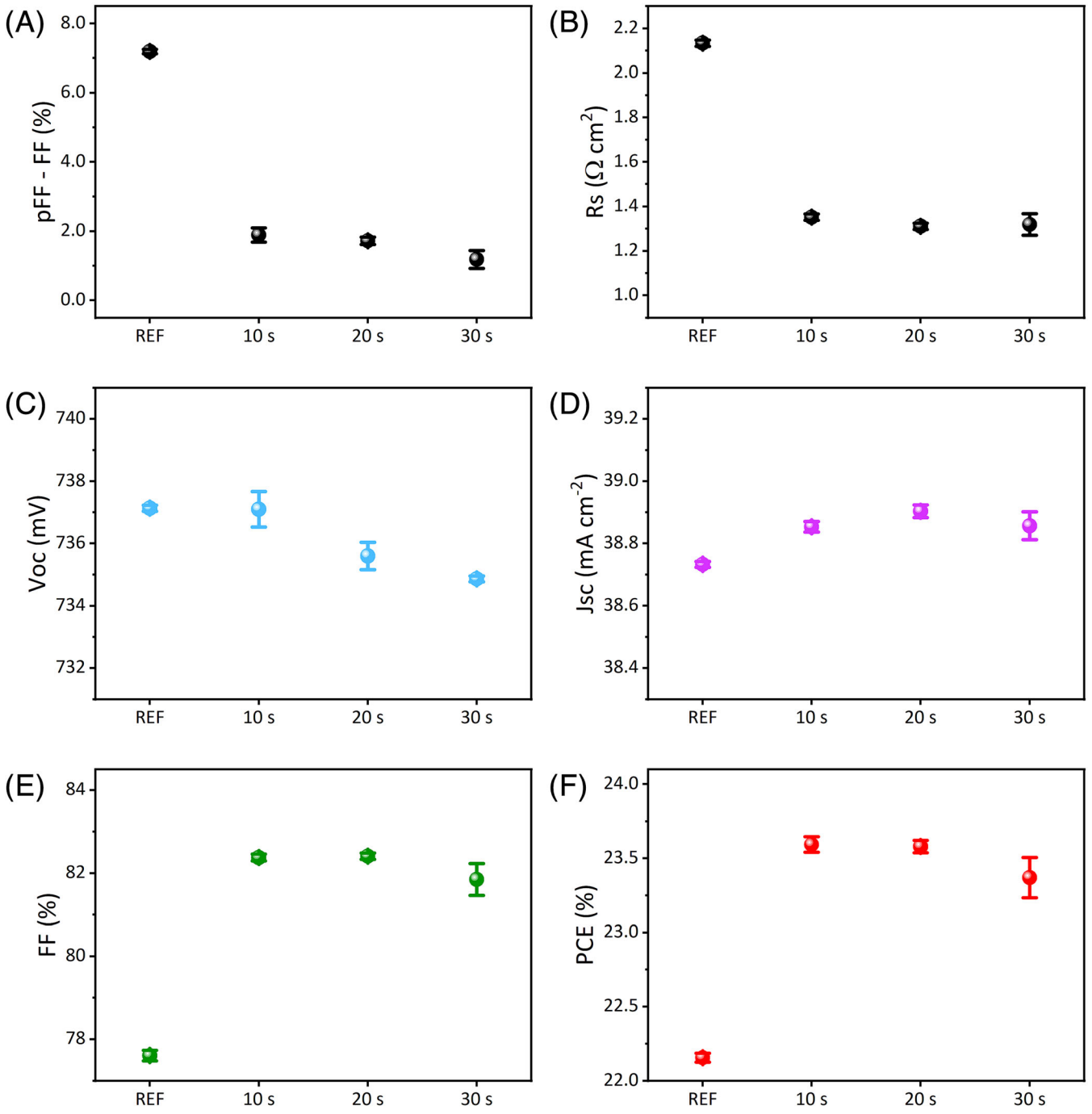

FIGURE 3 Performance of SHJ solar cells with different CO_2 PT duration, (A) p*FF*-*FF*, (B) R_s, (C) V_{OC}, (D) J_{SC}, (E) *FF*, and (F) *PCE*. The values are average values from three pieces of 6-in. rear-emitter SHJ solar cells (~244 cm^2), and error bars represent the standard deviation.

with a 10 s CO_2 PT process significantly decreases but does not decrease further with additional CO_2 PT duration.

Output parameters of 6-in. SHJ solar cells (~244 cm^2) with different CO_2 PT duration are plotted in Figure 3C–F. With the increase of CO_2 PT duration, V_{OC} decreases gradually, in good agreement with iV_{OC}, dark *J*-*V* and R_{sh}, stemming from increasing density states and passivation degradation. However, it has a gain about 0.15 mA cm^{-2} in short-circuit current density (J_{SC}), and more importantly, *FF* boosts from 77.61% to 82.37% (10 s) and 82.41% (20 s) due to a significant decrease in R_s. When CO_2 PT duration is added to 30 s, *FF* decreases to 81.85%. Since both R_s and R_{sh} take effects on *FF* of SHJ solar cells,[31] this trend means that the gain of R_s reduction on *FF* is much greater than the loss of R_{sh} reduction, but the loss of *FF* cannot be ignored in case of overlong CO_2 PT. Thanks to improvement of *FF*, *PCE* increases from 22.16% to 23.59% or 23.58% with a 10 or 20 s CO_2 PT duration and then decreases to 23.37% with a 30 s CO_2 PT

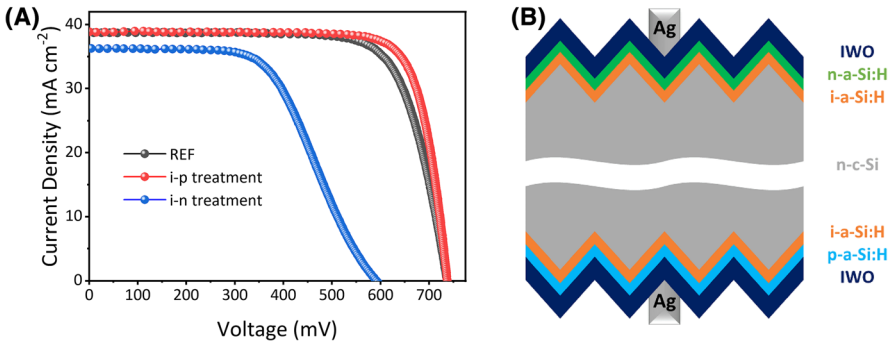

FIGURE 4 (A) One-Sun *J-V* curve of SHJ solar cells with a CO_2 PT at different sides. (B) The schematic diagram of the 6-in. rear-emitter SHJ solar cell

process. The *J-V* curve under simulated AM 1.5G solar irradiation of the best device named i-p treatment is plotted in Figure 4A. The best device undergoing a 10 s CO_2 PT process shows the highest *PCE* of 23.64% with a J_{SC} of 38.87 mA cm^{-2}, a V_{OC} of 737.6 mV, and an *FF* of 82.45%.

Moreover, we also apply CO_2 PT to the interface of i-n stacks of SHJ solar cells. The *J-V* curve under simulated AM 1.5G solar irradiation of the best device named i-n treatment is plotted in Figure 4A. The *J-V* curve shows S-shape, and the device performance shows an overall degradation; that is, V_{OC}, J_{SC}, *FF*, and *PCE* are 591.9 mV, 36.29 mA cm^{-2}, 58.81%, and 12.63%, respectively. The poor performance indicates the selective electron transmission of the device is seriously hindered. This further proves that the interface with dipoles and defect states caused by CO_2 PT helps hole transport but hinders electron transport.

4 | CONCLUSION

In conclusion, we demonstrate that the CO_2 PT after the deposition of i-a-Si:H film injects O atoms to amorphous silicon network and then getters H atoms from the plasma of SiH_4 and H_2 during the p-a-Si:H deposition. This leads to a longitudinal distribution of H and O atoms that creates a dipole moment. It reduces $WF_{surface}$ by 0.44 eV and causes the conduction band and the valence band to bend upwards and thus reduces the hole hopping distance and blocks electron transport. We also demonstrate that the CO_2 PT increases defect states. To some extent, more defect states reduce passivation performance, which causes the decrease of R_{sh} and V_{OC}, but are beneficial for hole to hop through the i-a-Si:H layer. Even though increasing the CO_2 PT duration from 10 to 30 s leads to some performance loss, the key thing is that even at 30 s, there is a clear benefit to the solar cell efficiency. As a whole consequence, a 10 s CO_2 PT process at the i/p interface of SHJ solar cells gains their *FF* by 6.13% and *PCE* by 6.45% relatively.

ACKNOWLEDGEMENTS

This work was supported by the National Natural Science Foundation of China (62004208, T2322028 62074153), the Science and Technology Commission of Shanghai Municipality (22ZR1473200), the Foundation of the Key Laboratory of National Defense for Science and Technology of China (61428040202), and the Research on Key technologies of high efficiency ultra-thin heterojunction solar cell and module (HNKJ22-H154). We thank Zhijun Jia for the EIS measurements and Bo Wang for the Raman spectra measurements.

DATA AVAILABILITY STATEMENT

The data that support the findings of this study are available from the corresponding author upon reasonable request.

CONFLICT OF INTEREST STATEMENT

The authors declare no conflict of interest.

ORCID

Shenglei Huang https://orcid.org/0000-0003-2345-5668
Yinuo Zhou https://orcid.org/0000-0002-1607-3226
Junlin Du https://orcid.org/0000-0002-7838-0045
Anjun Han https://orcid.org/0000-0003-1216-5577
Jian Yu https://orcid.org/0000-0001-6824-064X

REFERENCES

1. Wolf SD, Descoeudres A, Holman ZC, Ballif C. High-efficiency silicon heterojunction solar cells: a review. *Green*. 2012;2(1):7-24. doi:10.1515/green-2011-0018
2. Taguchi M, Yano A, Tohoda S, et al. 24.7% record efficiency HIT solar cell on thin silicon wafer. *IEEE J Photovoltaics*. 2014;4(1):96-99. doi:10.1109/JPHOTOV.2013.2282737
3. Haschke J, Seif JP, Riesen Y, et al. The impact of silicon solar cell architecture and cell interconnection on energy yield in hot & sunny climates. *Energ Environ Sci*. 2017;10(5):1196-1206. doi:10.1039/C7EE00286F
4. Liu W, Shi J, Zhang L, et al. Light-induced activation of boron doping in hydrogenated amorphous silicon for over 25% efficiency silicon solar cells. *Nat Energy*. 2022;7(5):427-437. doi:10.1038/s41560-022-01018-5
5. Green MA, Dunlop ED, Siefer G, et al. Solar cell efficiency tables (Version 61). *Progr Photovoltaics: Res Applic*. 2022;31(1):3-16. doi:10.1002/pip.3646
6. Lin H, Yang M, Ru X, et al. Silicon heterojunction solar cells with up to 26.81% efficiency achieved by electrically optimized nanocrystalline-silicon hole contact layers. *Nat Energy*. 2023;8(8):789-799. doi:10.1038/s41560-023-01255-2
7. Feng C, Wang X, He Z, Cao Y. Formation mechanism of PFN dipole interlayer in organic solar cells. *Solar RRL*. 2021;5(4):2000753. doi:10.1002/solr.202000753
8. Choi H, Kim HB, Ko SJ, Kim JY, Heeger AJ. An organic surface modifier to produce a high work function transparent electrode for high

performance polymer solar cells. *Adv Mater*. 2015;27(5):892-896. doi:10.1002/adma.201404172
9. Ok SA, Jo B, Somasundaram S, et al. Management of transition dipoles in organic hole-transporting materials under solar irradiation for perovskite solar cells. *Nat Commun*. 2018;9(1):4537. doi:10.1038/s41467-018-06998-1
10. Canil L, Cramer T, Fraboni B, et al. Tuning halide perovskite energy levels. *Energ Environ Sci*. 2021;14(3):1429-1438. doi:10.1039/D0EE02216K
11. Ros E, Barquera Z, Ortega PR, et al. Improved electron selectivity in silicon solar cells by cathode modification with a dipolar conjugated polyelectrolyte interlayer. *ACS Appl Energy Mater*. 2019;2(8):5954-5959. doi:10.1021/acsaem.9b01055
12. Ji W, Allen T, Yang X, Zeng G, de Wolf S, Javey A. Polymeric electron-selective contact for crystalline silicon solar cells with an efficiency exceeding 19%. *ACS Energy Lett*. 2020;5(3):897-902. doi:10.1021/acsenergylett.0c00110
13. Ros E, Tom T, Rovira D, et al. Expanding the perspective of polymeric selective contacts in photovoltaic devices using branched polyethylenimine. *ACS Appl Energy Mater*. 2022;5(9):10702-10709. doi:10.1021/acsaem.2c01422
14. Soman A, Nsofor U, Das U, Gu T, Hegedus S. Correlation between in situ diagnostics of the hydrogen plasma and the Interface passivation quality of hydrogen plasma post-treated a-Si:H in silicon heterojunction solar cells. *ACS Appl Mater Interfaces*. 2019;11(17):16181-16190. doi:10.1021/acsami.9b01686
15. Zhao Y, Mazzarella L, Procel P, et al. Doped hydrogenated nanocrystalline silicon oxide layers for high-efficiency c-Si heterojunction solar cells. *Progr Photovoltaics: Res Applic*. 2020;28(5):425-435. doi:10.1002/pip.3256
16. Zhang L, Guo W, Liu W, et al. Investigation of positive roles of hydrogen plasma treatment for interface passivation based on silicon heterojunction solar cells. *J Phys D Appl Phys*. 2016;49(16):165305. doi:10.1088/0022-3727/49/16/165305
17. Jiang K, Yang Y, Yan Z, et al. Balance of efficiency and stability of silicon heterojunction solar cells. *Solar Energy Mater Solar Cells*. 2022;243:111801. doi:10.1016/j.solmat.2022.111801
18. Muralidharan P, Goodnick SM, Vasileska D. Modeling of transport in carrier-selective contacts in silicon heterojunction solar cells. *Progr Photovoltaics: Res Applic*. 2022;30(5):490-502. doi:10.1002/pip.3515
19. Schulze TF, Korte L, Conrad E, Schmidt M, Rech B. Electrical transport mechanisms in a-Si:H/c-Si heterojunction solar cells. *J Appl Phys*. 2010;107(2):023711. doi:10.1063/1.3267316
20. Lucovsky G, Yang J, Chao SS, Tyler JE, Czubatyj W. Oxygen-bonding environments in glow-discharge-deposited amorphous silicon-hydrogen alloy films. *Phys Rev B*. 1983;28(6):3225-3233. doi:10.1103/PhysRevB.28.3225
21. El-Sayed AM, Watkins MB, Grasser T, Afanas'ev VV, Shluger AL. Hydrogen-induced rupture of strained Si horizontal line O bonds in amorphous silicon dioxide. *Phys Rev Lett*. 2015;114(11):115503. doi:10.1103/PhysRevLett.114.115503
22. Perkins GGA, Austin ER, Lampe FW. The 147-nm photolysis of monosilane. *J am Chem Soc*. 1979;101(5):1109-1115. doi:10.1021/ja00499a010
23. Leung TC, Kao CL, Su WS, Feng YJ, Chan CT. Relationship between surface dipole, work function and charge transfer: some exceptions to an established rule. *Phys Rev B*. 2003;68(19):195408. doi:10.1103/PhysRevB.68.195408
24. Wang B, Li H, Dai Q, et al. Robust molecular dipole-enabled defect passivation and control of energy-level alignment for high-efficiency perovskite solar cells. *Angew Chem Int Ed Engl*. 2021;60(32):17664-17670. doi:10.1002/anie.202105512
25. Mazzarella L, Kirner S, Gabriel O, et al. Nanocrystalline silicon emitter optimization for Si-HJ solar cells: substrate selectivity and CO2 plasma treatment effect. *Phys Status Solidi (a)*. 2017;214(2):1532958. doi:10.1002/pssa.201532958
26. Jiang Y. CO2 plasma treatment to promote crystallinity of p-type emitter layer for the silicon heterojunction solar cells. *J Mater Sci Mater Electron*. 2022;33(7):3670-3675. doi:10.1007/s10854-021-07559-x
27. Michl B, Impera D, Bivour M, Warta W, Schubert MC. Suns-PLI as a powerful tool for spatially resolved fill factor analysis of solar cells. *Progr Photovoltaics: Res Applic*. 2014;22(5):581-586. doi:10.1002/pip.2293
28. Taguchi M, Maruyama E, Tanaka M. Temperature dependence of amorphous/crystalline silicon heterojunction solar cells. *Jpn J Appl Phys*. 2008;47(2):814-818. doi:10.1143/JJAP.47.814
29. Muralidharan P, Goodnick SM, Vasileska D. Kinetic Monte Carlo simulation of transport in amorphous silicon passivation layers in silicon heterojunction solar cells. *J Comput Electron*. 2019;18(4):1152-1161. doi:10.1007/s10825-019-01379-3
30. Greulich J, Glatthaar M, Rein S. Fill factor analysis of solar cells' current-voltage curves. *Progr Photovoltaics: Res Applic*. 2010;18(7):511-515. doi:10.1002/pip.979
31. Khanna A, Mueller T, Stangl RA, Hoex B, Basu PK, Aberle AG. A fill factor loss analysis method for silicon wafer solar cells. *IEEE J Photovoltaics*. 2013;3(4):1170-1177. doi:10.1109/JPHOTOV.2013.2270348

SUPPORTING INFORMATION

Additional supporting information can be found online in the Supporting Information section at the end of this article.

How to cite this article: Huang S, Yang Y, Li J, et al. Dipoles and defects caused by CO_2 plasma improve carrier transport of silicon solar cells. *Prog Photovolt Res Appl*. 2024;32(5):283-290. doi:10.1002/pip.3761